Zika Virus Attenuation by Codon Pair Deoptimization Induces Sterilizing Immunity in Mouse Models

Penghui Li[a,b], Xianliang Ke[a], Ting Wang[a,c], Zhongyuan Tan[a], Dan Luo[a], Yuanjiu Miao[a], Jianhong Sun[a], Yuan Zhang[a], Yan Liu[a], Qinxue Hu[d], Fuqiang Xu[c], Hanzhong Wang[a]*, Zhenhua Zheng[a]*

[a] CAS Key Laboratory of Special Pathogens and Biosafety, Center for Emerging Infectious Diseases, Wuhan Institute of Virology, Chinese Academy of Sciences, Wuhan 430071, PR China;

[b] University of Chinese Academy of Sciences, Beijing 100049, PR China;

[c] State Key Laboratory of Magnetic Resonance and Atomic and Molecular Physics, Key Laboratory of Magnetic Resonance in Biological Systems, Wuhan Center for Magnetic Resonance, Wuhan Institute of Physics and Mathematics, Chinese Academy of Sciences, Wuhan 430071, P.R. China;

[d] State Key Laboratory of Virology, Wuhan Institute of Virology, Chinese Academy of Sciences, Wuhan 430071, China

Running Head: ZIKV Attenuation by Codon Pair Deoptimization

***Corresponding Authors**:

Dr. Hanzhong Wang, Email: wanghz@wh.iov.cn ;

Dr. Zhenhua Zheng, Email: zhengzh@wh.iov.cn .

Word count:

Abstract: 215 Main text: 5776

ABSTRACT

Zika virus (ZIKV) infection during the large epidemics in the Americas is related to congenital abnormities or fetal demise. To date, there is no vaccine, antiviral drug, or other modality available to prevent or treat Zika virus infection. Here we designed novel live attenuated ZIKV vaccine candidates using a codon pair deoptimization strategy. Three codon pair-deoptimized ZIKVs (Min E, Min NS1, and Min E+NS1) were *de novo* synthesized, and recovered by reverse genetics, containing large amounts of underrepresented codon pairs in E gene and/or NS1 gene. Amino acid sequence was 100% unchanged. The codon pair-deoptimized variants had decreased replication fitness in Vero cells (Min NS1 >> Min E > Min E+NS1), replicated more efficiently in insect cells than in mammalian cells, and demonstrated diminished virulence in a mouse model. In particular, Min E+NS1, the most restrictive variant, induced sterilizing immunity with a robust neutralizing antibody titer, and a single immunization achieved complete protection against lethal challenge and vertical ZIKV transmission during pregnancy. More importantly, due to the numerous synonymous substitutions in the codon pair-deoptimized strains, reversion to wild-type virulence through gradual nucleotide sequence mutations is unlikely. Our results collectively demonstrate that ZIKV can be effectively attenuated by codon pair deoptimization, highlighting the potential of Min E+NS1 as a safe vaccine candidate to prevent ZIKV infections.

IMPORTANCE

Due to unprecedented epidemics of Zika virus (ZIKV) across the Americas and the unexpected clinical symptoms including Guillain-Barré syndrome, microcephaly and other birth defects in human, there is an urgent need for ZIKV vaccine development.

Journal of Virology JVI Journal of Virology

Here, we provided the first attenuated versions of ZIKV with two important genes (E and/or NS1) that were subjected to codon pair deoptimization. Compared to parental ZIKV, the codon pair-deoptimized ZIKVs were mammalian-attenuated, and preferred insect to mammalian Cells. Min E+NS1, the most restrictive variant, induced sterilizing immunity with a robust neutralizing antibody titer, and achieved complete protection against lethal challenge and vertical virus transmission during pregnancy. More importantly, the massive synonymous mutational approach made it impossible to revert to wild-type virulence. Our results have proven the feasibility of codon pair deoptimization as a strategy to develop live-attenuated vaccine candidates against flavivirues like ZIKV, Japanese encephalitis virus and West Nile virus.

KEYWORDS Codon pair bias, Zika, E, NS1, deoptimization, vaccine

INTRODUCTION

Zika virus (ZIKV) is an enveloped virus that belongs to the *Flaviviridae* family (1). ZIKV was first isolated from the blood of a febrile rhesus macaque in 1947 in the Zika forest of Uganda (2), and has become a major public health risk globally driven by the current unprecedented epidemics of ZIKV across the Americas (3-5). ZIKV is usually associated with asymptomatic infections or mild febrile illness accompanied by rash conjunctivitis in human (6); however, during the large epidemics in the Americas, ZIKV infection tends to cause more severe clinical manifestations including Guillain-Barre' syndrome (GBS), meningoencephalitis, microcephaly and other birth defects (3, 4, 7). The virus is mainly transmitted by Aedes mosquitoes, but human-to-human transmission through sexual and vertical routes have also been reported, which was different from most other flaviviruses (8, 9). The efficient transmission and comparatively limited antiviral therapeutic options have aggravated the current panic over ZIKV. To date, there is no effective licensed vaccine or antiviral treatment against ZIKV infection, although several vaccine candidates have been described including formalin inactivated vaccines (10, 11), live attenuated vaccines (12), genetic vaccines (11, 13-17), and virus-like particle (VLP) vaccines (18, 19). Therefore, new options for the development of ZIKV vaccine are needed.

ZIKV genome is a single plus-strand RNA of approximately 11 kb in length and contains a single open reading frame (ORF) encoding a polyprotein that is subsequently cleaved by cellular and viral proteases into three structural proteins (C, prM, and E) and seven nonstructural proteins (NS1, NS2A, NS2B, NS3, NS4A, NS4B, and NS5) (20, 21).The structural proteins form viral particles, and mediate attachment and entry of

ZIKV into host cells, while the nonstructural proteins are engaged in viral genome replication, virus assembly, and evasion of the host innate immune response (20, 22, 23). Specifically, the envelope (E) protein is considered as a major determinant for ZIKV pathogenesis, and is involved in modulating the viral infection cycle (24). Although not being a component of viral particles, NS1 plays an essential role in viral RNA replication as well as in host immune recognition and evasion (25, 26). Hence, the multifunctional roles of E and NS1 gene products were regarded as ideal targets for attenuation to create novel live attenuated ZIKV vaccines.

Codon pair bias is interpreted as the unequal frequency in the usage of synonymous codon pairs in certain species (27-29). Based on the algorithm to quantify codon pair bias, every codon pair harbors a codon pair score (27, 28). Codon pairs with positive codon pair scores are statistically overrepresented, which may indicate that they are preferred by the organism, while the others with negative codon pair scores are underrepresented (28, 30). For instance, GCCGAA (codon pair score=-1.717) is strongly underrepresented and is used only one-seventh as frequently as GCAGAG (codon pair score=0.411), even though it contains GCC, the optimal Ala codon (27). The codon pair deoptimization, also known as synthetic attenuated virus engineering (SAVE), is a novel technique for viral attenuation by increasing the presence of underrepresented codon pairs (27, 31) In contrast, another attenuation strategy, codon deoptimization has also generated by introducing the least-preferred codons for the majority of the amino acid residues of the target genes (32, 33). Codon pair-deoptimized strains harbor identical amino acid sequences conserving the same repertoire of epitopes as the WT pathogen which may provide favorable immunogenicity and protective immunity, and contain numerous synonymous substitutions which could make the generation of virulent revertants

unlikely (34). Remarkably, the processes of codon pair deoptimization and codon deoptimization are often accompanied by the increases in CpG and UpA dinucleotide frequencies (28, 35, 36). CpG and UpA dinucleotides are rare in mammalian genes (37, 38) and eukaryotic RNA viruses (39, 40), as do the codon pairs with a central xxCpGxx or xxUpAxx generally (28, 30). A raised xxCpGxx content may induce an innate immune response in certain cells, which could decrease the replicative fitness of intracellular virus (41), while the xxUpAxx abundance is deemed to reduce mRNA stability (42). To date, codon deoptimization has been used to attenuate polio virus, respiratory syncytial virus, foot-and-mouth disease virus, arenavirus, and influenza virus (32, 33, 41, 43-46), and the codon pair deoptimization strategy has also been used to generate attenuated polio virus, respiratory syncytial virus, vesicular stomatitis virus, porcine reproductive and respiratory syndrome virus, dengue virus, and influenza virus (27, 28, 30, 31, 47-49).

In this study, three codon pair-deoptimized ZIKVs were designed, *de novo* synthesized, and recovered by reverse genetics. All the codon pair-deoptimized ZIKVs were attenuated to different extents in Vero cells (a mammalian cell line), but were not in C6/36 mosquito cells. Like their phenotype *in vitro*, codon pair-deoptimized ZIKVs were attenuated *in vivo*, and were also shown to conserve potent immunogenicity that completely protected vaccinated mice from lethal challenge and vertical virus transmission during pregnancy. These results raise the possibility of using codon pair deoptimization for the generation of novel live-attenuated ZIKV vaccine candidates.

RESULTS

Generation of codon pair-deoptimized ZIKVs. Because the codon pair biases between humans and mosquitoes are poorly correlated (28), the codon pair scores of the

E and NS1 genes of an Asian lineage Zika virus，SZ-WIV01 were reduced deeply according to the human codon pair bias table, but not according to the mosquito table (28). As is shown in Table 1, a total of 363 synonymous mutations were introduced in the specified E coding region, in which deoptimized human codon pair score ranged from 0.0336 to -0.5741, whereas the change was minimal for the mosquito codon pair score. The same thing happened in the NS1 coding region, with the average human codon pair score being reduced from 0.0059 to -0.5162 and the change being minimal for the mosquito codon pair score. In consideration of the potential impact on virus attenuation, the increases in the frequency of XXCpGXX and XXUpAXX were also calculated. As shown in Table 2, all the codon-pair deoptimized segments possess significantly more xxCpGxx (294%–455% increase) or xxUpAxx (185%–371% increase) dinucleotides than the WT counterparts. The codon pair-deoptimized sequences presented in this paper have been submitted to GenBank: WT, MH055376; Min E, MH055377; Min NS1, MH055378; Min E+NS1, MH055379.

The full-length ZIKVwt cDNA clone was constructed using reverse genetics methods (see Materials and Methods). ZIKVwt was recovered by transfection of it into Vero cells. Based on the full-length ZIKVwt cDNA clone, we designed and generated, by reverse genetics, three synthetic codon pair-deoptimized ZIKVs, named Min E, Min NS1, and Min E+NS1, in which various genome regions were subjected to codon pair deoptimization (Fig. 1). This enabled comparisons of the biological properties, pathogenicity and immunogenicity of the WT and codon pair-deoptimized viruses *in vitro* and *in vivo*.

Growth properties of codon pair-deoptimized ZIKVs *in vitro*. Vero cells and C6/36 cells were used to analyze the replicative properties of codon pair-deoptimized ZIKVs with each virus at the same moi of 0.01. In Vero cells, Min E as well as Min E+NS1 had a poor replication (Fig. 2A-B and Fig. 3). As for Min NS1, although its endpoint titers reached comparable levels to that of ZIKVwt, it displayed delayed replication kinetics; Min NS1 had reduced levels of viral RNA at 1 and 2 dpi ($p<0.01$) (Fig. 2A), and lower infectious titers at 3 and 4 dpi ($p<0.01$) (Fig. 2B) compared with WT virus. In addition, the average size of infectious foci decreased in the order WT, Min NS1, Min E and Min E+NS1 in Vero cells (Fig. 2G). These results indicated that the replication of the codon pair-deoptimized variants in Vero cells dramatically decreases (replication fitness: Min NS1 >> Min E > Min E+NS1).

In C6/36 cells, all of the codon pair-deoptimized viruses as well as ZIKVwt reached the maximum viral loads of $>2\times10^{10}$ copies/ml at 8dpi (Fig. 2C). Compared with ZIKVwt, Min E+NS1 even displayed enhanced RNA replication kinetics before 4dpi (Fig. 2C), although there were no significant differences. Immunostaining focus assay was carried out to determine the infectious titers. The maximal titers of Min NS1 and Min E between 7 and 8 dpi were comparable to that of the WT virus, however, they displayed delayed replication kinetics. Min NS1 had lower infectious titers at 1, 3 and 4 dpi ($p<0.05$) (Fig. 2D), and Min E had reduced level of infectious titers at 1, 3, 4, 5 and 6 dpi ($p<0.05$) (Fig. 2D). The infectious titers of Min E+NS1 decreased stepwise at all time points ($p<0.05$) (Fig. 2D).

Next, multipassage analysis was performed to test the passage stability of ZIKVs. Both ZIKVwt and Min NS1 reached high viral loads (Fig. 2E) and were capable of

developing infectious foci in Vero cells (Fig. 2F) from P1 to P5. Min E as well as Min E+NS1 was nonviable in Vero cells by the fourth passage and the second passage, respectively (Fig. 2E-F).

Diminished virulence of codon pair-deoptimized ZIKVs in AG6 mice. An AG6 mouse model was used to evaluate the diminished virulence of codon-pair deoptimized ZIKVs. Four-week-old AG6 mice were infected with different doses of ZIKVwt or codon pair-deoptimized ZIKVs through the i.p. route. Under our experimental conditions, ZIKVwt was highly virulent in these AG6 mice, with an LD50 of 1.78 PFU. Min NS1 was slightly attenuated in mice with a ~1.7-fold increase in LD50 compared with ZIKVwt (Table 3). Dramatic attenuations were observed with Min E and Min E+NS1, revealing ~1000-fold and ~2000-fold increases in MLD50, respectively, compared with ZIKVwt (Table 3). The order of attenuations in the animals (Min E+NS1 >Min E >> Min NS1) was consistent with the order of attenuations in tissue culture cells.

Comparative analysis of pathogenicity. AG6 mice were infected with 100IFU of either ZIKVwt or codon pair-deoptimized ZIKVs, and monitored for 28 days for weight loss (Fig. 4A), and mortality (Fig. 4B). Mice were also periodically euthanized to perform virus detection in various organs (at day 3 and 7dpi) (Fig. 5, 6A-B) and sera (at 3 and 6dpi) (Fig. 6C). As expected, codon pair-deoptimized ZIKVs showed levels of pathogenicity different from those for ZIKVwt. Mice infected with Min E+NS1 shared comparable kinetics of weight gain with that of mock-treated mice (Fig. 4A), and all survived (Fig. 4B). In contrast, the survival rates of ZIKVwt, Min NS1 and Min E group were 0%, 16.7% and 83.3%, respectively. Immunohistochemistry (IHC) staining with brain tissue sections showed a wide distribution of E protein in mice infected with WT

196 virus, in contrast, it is difficult to detect the distribution of E protein in mice infected with
197 Min E+NS1 virus (Fig. 5).

198 The pathogenicity and virus load in sera as well as in infected organs are usually
199 positively correlated (12, 30), thus, viral titers in sera, heart, liver, spleen, lung, kidney,
200 brain, testes, uterus, ovary, eye, intestine and muscle were measured by qRT-PCR (Fig.
201 6A and 6C), and immunostaining focus assay (Fig. 6B). Min E+NS1 was nonviable in all
202 the tested organs except for spleen. The mean viral load of Min E+NS1 infected spleens
203 was $10^{2.17}$ copies/μg total RNA at 3 dpi, which was at least three orders of magnitude less
204 than that in their WT infected counterparts ($p<0.05$), and was reduced to $10^{1.28}$ copies/μg
205 total RNA at 7 dpi. The supernatants (homogenized Min E+NS1 infected spleens) were
206 not capable of developing infectious foci in Vero cells (Fig. 6B). In contrast, in ZIKVwt-
207 infected animals, viral RNA was widespread in all the tested organs up to 7 dpi (Fig. 6A),
208 which ultimately resulted in the death of all the remaining animals by 9 dpi (Fig. 4B).

209 **Immunogenicity and efficacy of codon pair-deoptimized ZIKVs in AG6 mice.**
210 To evaluate whether codon pair-deoptimized ZIKVs immunization elicited a B cell-
211 mediated humoral immunity, sera were collected 28 days postvaccination through the
212 retro-orbital sinus, and titers of ZIKV-specific neutralizing antibodies (NAb) were
213 measured by the $PRNT_{50}$ assay. Mice infected with the WT or codon pair-deoptimized
214 viruses were found to have comparable neutralizing antibody titers against the WT virus,
215 whereas the control mice did not develop a detectable $PRNT_{50}$ titer ($PRNT_{50}<10$) (Fig.
216 7A). To evaluate cellular immune responses in AG6 mice, on day 28 postimmunization,
217 ZIKV-specific T cells from the spleen were restimulated with heat-inactivated WT virus
218 in vitro, and analyzed by an IFN-γ ELISpot assay. The results showed that the average

IFN-γ levels secreted from the Min E+NS1-immunized group were significantly higher than that of the mock-immunized group ($p<0.01$) (Fig. 7B).

The mice were then challenged with 10^4 PFU of WT virus intraperitoneally, representing an approximately 5500-fold MLD50 of ZIKVwt. All vaccinated animals survived without detectable peripheral viremia and any signs of disease (weight loss, ruffled fur, hindlimb paralysis, hunched posture, or lethargy) through day 14 (Fig. 8A-C), whereas the sham-vaccinated mice produced a mean viremia of $(5.2 \pm 4.0) \times 10^8$ copies/ml on day 3 after challenge (Fig. 8C) and died by 10 days after challenge (Fig. 8B). Furthermore, high titers of neutralizing antibodies in challenged mice were also detected (Fig. 8D). Taken together, a single-dose vaccination of the Min E+NS1 virus can elicit a robust immune response that fully protects AG6 mice against a subsequent lethal challenge. On day 28 after challenge, we measured the neutralization titers of the mouse sera again; notably, the postchallenge neutralization titers were equivalent to the prechallenge neutralization titers

To determine if Min E+NS1 immunization could protect pregnant AG6 mice, we mated immunized AG6 female mice with 8-week-old naïve AG6 male mice at day 32 post immunization and challenged the pregnant mice with 10^4 PFU of WT virus at embryo day 6 (E6) (Fig. 9A). As expected, high titers of neutralizing antibodies in pregnant mice were detected at day 1 before challenge (Fig. 9B). Following WT challenging, Min E+NS1 immunized had no signs of disease (weight loss, ruffled fur, hindlimb paralysis, hunched posture, or lethargy) throughout the experiment. PBS-immunized mice developed high levels of maternal viremia, however, Min E+NS1 immunized mice had no detectable maternal viremia (Fig. 9C). All PBS-immunized mice died without delivery, in contrast, all Min E+NS1 vaccinated dams successfully delivered

243 the healthy pups at term with normal viability (Fig. 9D). Modest low levels of maternal
244 neutralization antibody were even detected in the sera of pups at the 21th day after birth
245 (Fig. 9D). Collectively, preconception maternal immunity induced by Min E+NS1
246 immunization efficiently protected AG6 mice during pregnancy, and prevented viral
247 transmission to the fetus.

248 **DISCUSSION**

249 We have investigated the strategy of codon pair deoptimization as a means to
250 develop novel attenuated versions of ZIKV, a pathogenic virus that caused GBS,
251 meningoencephalitis, microcephaly and other birth defects in human (3, 4, 7). Viruses
252 harboring deoptimized codon pairs in the E gene, NS1 gene, and E+NS1 gene were
253 designed, rescued, and proven to be attenuated to different extents *in vitro* and *in vivo*. It
254 should be pointed out that the most attenuated Min E+NS1 virus possessed potential to
255 the generic development of live attenuated vaccines that produced robust
256 immunogenicity, provided complete protection against a lethal challenge of ZIKV,
257 protected AG6 mice during pregnancy, and prevented viral transmission to the fetus with
258 a single dose.

259 As far as we know, several live-attenuated ZIKV vaccines have been reported (12,
260 50). Shan et al has generated a recombinant live-attenuated ZIKV vaccine candidate by
261 deletion of 10-nts in the viral 3'-UTR by reverse genetics (12), while Li et al develops
262 and characterizes a recombinant chimeric ZIKV vaccine candidate expressing the prM-E
263 proteins of ZIKV using the licensed Japanese encephalitis live-attenuated vaccine SA14-
264 14-2 as the genetic backbone (50). Using strategy of codon pair deoptimization, our
265 attenuated Min viruses express identical whole protein sequences conserving an intact

antigenic repertoire. Moreover, due to the large number of mutations introduced, these attenuated Min viruses are unlikely to develop virulent revertants through gradual nucleotide sequence mutations.

Several mechanisms appeared to be related to the attenuation in ZIKV Min variants caused by rare codon pairs. The major effect of codon pair deoptimization should be decreased efficiency of translation in a context-dependent manner (27, 30, 32). A string of "rare" codon pairs compound the difficulties of reading through by the ribosome, resulting in less precursor proteins per mRNA. Other parameters coordinated with the translation elongation rate, such as ribosomal stalling, premature dissociation of the translation initiation complex, protein processing, folding, and/or stability, may also be involved (28, 33, 51). Additionally, the increase of CpG and UpA dinucleotides can also play important roles in RNA virus attenuation (28, 35, 36, 52, 53). Mammalian genomes and eukaryotic RNA viruses exhibit marked CpG/UpA suppression (37-40). The raised dinucleotide composition may induce an innate immune response in host cells (41, 54), and/or reduce mRNA stability (42). The recoded segments with rare codon pairs are generally associated with an enrichment of CpG and UpA dinucleotides (28, 30, 41, 43, 44). In agreement, we found that all the codon pair-deoptimized segments possess significantly more xxCpGxx or xxUpAxx dinucleotides than the WT counterparts. Codon pair bias has been suggested to be a direct consequence of CpG/UpA dinucleotide bias (55), and the rise of CpG/UpA dinucleotides may be a key genetic contributor to virus attenuation by codon pair deoptimization (56), although this has been disputed (28, 57). Another finding is that the effect of codon pair usage or dinucleotide frequencies on translation is minor or nonexistent (43, 44, 52, 56), which warrants further investigation. In conclusion, it is difficult to distinguish the two effects (the increased CpG and UpA

dinucleotides or the increased frequency of disfavored codon pairs) that mediate the attenuation in ZIKV Min variants in this study.

Each of the codon pair-deoptimized ZIKVs replicated less efficiently in Vero cells than the WT virus. Min E+NS1 was the most restricted codon pair-deoptimized mutant, exhibited the smallest infectious foci (Fig. 2G), the slowest replication kinetics, and the lowest peak titer (Fig. 2A-B), informing that it involves an "additive" relationship of the effect of recoded genomes, with significantly more rare codon pairs, as found with poliovirus (27), or significantly more CpG/UpA dinucleotides than those in Min E and Min NS1 (41, 42, 54). Min NS1 was less restricted in Vero cells than Min E. The seemingly counterintuitive result may be explained by the amount of codon pair changes introduced in the corresponding segments or inappropriate molar ratios of proteins relative to mRNAs, and implied that the suboptimal of NS1 could be tolerated to some extent. A key result was the observation that all the three codon pair-deoptimized ZIKVs replicated more efficiently in C6/36 cells, when compared with Vero cells (Fig. 2). The alteration of cell tropism was due to the introduction of hundreds of underrepresented human codon pairs. Because there was a poor correlation between humans and mosquitoes codon pair preference, the accumulation of underrepresented human codon pairs would not drift the cumulative codon pair score too far according to the insect table (28). One of the potential benefits is practicability of launching platform for high-yield production of attenuated ZIKV vaccine in insect cell systems, such as Sf9 and Sf21 cell lines. Although the raised CpG/UpA dinucleotide composition profoundly reduced the replication ability of RNA virus in mammalian cells, it is uncertain whether this is also true in mosquito cells. Therefore, the fact that codon pair-deoptimized ZIKVs prefer mosquito to mammalian cells may not be associated with the differences in sensing

314 CpG/UpA in the deoptimized viruses compared to WT virus.

315 Mice deficient in the type I and type II IFN (IFN α/β/γ) receptors are extremely
316 susceptible to ZIKV infection and display severe disease signs including hind limb
317 weakness, paralysis, and death, which provide a platform for identifying determinants of
318 ZIKV virulence and testing the efficacy of antivirals and vaccines (8, 58-60). Thus, AG6
319 mice lacking the type I and type II IFN (IFN α/β/γ) receptors were used in the study. As
320 expected, diminished virulence was clearly determined in the codon pair-deoptimized
321 variants (Table 3), revealing ~1.7-fold (Min NS1), ~1000-fold (Min E), and ~2000-fold
322 (Min E+NS1) increases in MLD50 compared with WT virus. We hypothesize that this
323 observation is related to viral attenuation in tissue culture cells, although viral attenuation
324 in tissue culture cells do not (necessarily) translate to that in animals (28). It is known that
325 ZIKV was associated with microcephaly, and caused testis damage (leading to male
326 infertility in mice) (7, 61, 62). In immunocompromised mouse model, ZIKV was
327 widespread in all the tested tissues including brain and testis (58, 59), which was also
328 present in our work (Fig. 6A). By contrast, Min E+NS1 was nonviable in all the tested
329 organs (the supernatant of homogenized spleens were not capable of developing
330 infectious foci, in spite of low-level detection of viral RNA). The observation suggested
331 that the risk of brain and testis damage is negligible. Despite high attenuation of Min
332 E+NS1 in the host, it induced high levels of neutralizing antibodies and IFN-γ in mice,
333 and conferred protection against lethal challenge with WT virus. In addition,
334 preconception maternal immunity induced by Min E+NS1 immunization is sufficient to
335 protect pregnant AG6 mice and their fetuses (Fig. 9). We hypothesize that the strong
336 protection was ascribed to that our codon pair-deoptimized viruses obtained repertoire of
337 epitopes identical to that of WT virus (amino acid sequence is 100% preserved). To data,

Min E+NS1 is the first attenuated version of flavivirus with two important genes that were subjected to codon pair deoptimization simultaneously, maintaining a balance between efficacy and safety.

In summary, we describe the first large-scale recoding of ZIKV, a flavivirus that belongs to a large family of mosquito-borne human pathogens. Min E+NS1 displayed the potential to develop into a promising live-attenuated vaccine candidate. Results from this study demonstrated the feasibility of rapid attenuation of ZIKV through the codon pair deoptimization strategy. The unparalleled advantage of the codon pair deoptimization strategy is that reversion to wild-type virulence is unlikely due to numerous synonymous substitutions without changing the amino acid sequence (34, 43). Thus, the codon pair deoptimization strategy would add the safety to the features of live attenuated viruses, which has a broad application in the development of vaccines for flavivirus and other important viruses.

MATERIALS AND METHODS

Ethics Statement. All experiments involving animals have been reviewed and approved by the Animal Care Committee of Wuhan Institute of Virology (Permit Number: WIVA07201603), in accordance with the animal ethics guidelines of the Chinese National Health and Medical Research Council (NHMRC).

Cells. African green monkey kidney epithelial cells (Vero; CCL-81; ATCC) were cultured in Dulbecco's modified Eagle's medium (DMEM; Invitrogen, Darmstadt, Germany) containing 10% fetal bovine serum (FBS; Life Technology, Australia), 100 U/ml penicillin and 100 μg/ml streptomycin, and maintained in 5% CO2 at 37°C. *Aedes albopictus* C6/36 cells (C6/36; CRL-1660; ATCC) were maintained in RPMI medium

1640 (Gibco, Carlsbad, CA, UK) containing 10% FBS in 5% CO2 at 28°C.

Design of Codon Pair-Deoptimized Sequences. E and NS1 genes were re-encoded by rearranging existing synonymous codons to minimize the cumulative codon pair scores according to the human codon pair bias table (27). The RNAfold software (63) was used to maintain the free energy of the folding of the RNA within a narrow range and to avoid large changes in secondary structure of the customized RNA as a consequence of codon re-arrangement. The mutated viral RNA segments were then synthesized commercially (Beijing Tsingke Biotech Co., Beijing, China).

Construction of ZIKV infectious clones (ICs). The Asian-lineage strain SZ-WIV01 was obtained from China Centre for General Virus Culture Collection (CCGVCC) (64). To generate the infectious cDNA of ZIKVwt, viral RNA was extracted from the parental virus by using TRIzol Reagent (TaKaRa, Dalian, China), and reverse transcribed by using PrimeScript^{TM} RT reagent kit (TaKaRa, Dalian, China) according to the respective manufacturers' instruction. Five PCR fragments covering the complete viral genome of ZIKV were amplified from the cDNA reverse transcribed. PCR fragment 1 containing nt 1-1590 of the genome was fused with CMV promoter and cloned into the low-copy-number plasmid pACYC177 at the KpnI and XhoI sites, yielding the subclone A. PCR fragment 2 containing nt 1532-3129, the beta-globin intron (nt. 857–989 in HaloTag CMV-neo vector pHTN, GenBank access JF920304), and PCR fragment 3 containing nt 3130-5309 were overlapped and cloned into pACYC177 at the AvrII and XhoI sites, yielding the subclone B. The previous study (65) provided some clues for the insertion site of the intron. PCR fragment 4 containing nt 5291-8588 was cloned into pACYC177 at the Cla I and Xho I sites, yielding the subclone C. PCR fragment 5 containing nt 8545-10942, hepatitis D virus ribozyme (HDVr) sequence, and SV40 polyA

were overlapped and cloned into pACYC177 at the SfiI and XhoI sites, yielding the subclone D. The four subclones were assembled step-by-step into a full-length infectious cDNA clone of ZIKVwt-FL as shown in Fig 1.

To generate the ICs of codon pair-deoptimized ZIKVs, the codon pair-deoptimized cassette (see above) was synthesized *de novo*, overlapped with flanking regions at either end and cloned into ZIKVwt-FL at the KpnI and ClaI sites, yielding ZIKV Min E-FL, ZIKV Min NS1-FL, and ZIKV Min E+NS1-FL, respectively (The designation "Min" signifies that genes were designed with minimized human codon pair score in this article). Before their transfection, all the ICs were verified using a restriction map and complete sequencing.

Rescue of infectious viruses and stock production. ICs were transfected into a 35 mm culture dish containing 80-90% confluent monolayers of Vero cells by lipofectamine 3000 (Life Technologies) in Opti-MEM (Life Technologies). The supernatant was harvested at 7 days post transfection (dpt, 4dpt for ZIKVwt), clarified by centrifugation and stored at -80°C.

Each virus was amplified in C6/36 cells with a multiplicity of infection (moi) of 1 in a 100 mm culture dish. Viral supernatants were harvested at 7 days post infection (dpi), clarified by centrifugation, aliquoted, and stored at -80°C. The nucleotide identities were confirmed by sequencing.

Virus growth kinetics. Sub-confluent (80%) cells in 100 mm culture dishes were infected at a moi of 0.01 in a volume of 2ml. After 1.5 h incubation at 37°C, cells were washed twice with 4ml of phosphate-buffered saline (PBS), and 8ml DMEM with 2% FBS (for Vero cells) or RPMI 1640 with 2% FBS (for C6/36 cells) was added. 800µL of cell supernatants were sampled at different time points post-infection, clarified by

centrifugation, aliquoted and stored until use. The virus particles were determined by real-time PCR (qRT-PCR), and infectious titers of the viruses were quantitatively analyzed using immunostaining focus assay.

Multipassage analysis. Each virus was passaged on Vero cells for five rounds. The virus derived from ZIKV ICs-transfected Vero cells was defined as the parental P0 virus and used for passaging. At each passage, a calculated moi of 0.01 was used to infect 35 mm culture dishes of sub-confluent (80%) cells. After 1.5 h incubation at 37°C, cells were washed three times with PBS, and 2ml DMEM with 2% FBS was added. At 4 dpi, viral supernatants were harvested, clarified, aliquoted, determined by qRT-PCR and immunostaining focus assay, and transferred to new 35 mm culture dishes containing naïve Vero cells. It should be noted that 10μl non-diluted stock solution of Min E and Min E+NS1 were used in P2-P5 passages.

Plaque assay and immunostaining focus assay. Virus titrations of ZIKVwt were determined with a plaque assays expressed as plaque forming units (PFU/ml). Briefly, Vero cells at 80% confluence in 24-well plates were inoculated with 100μl of 10-fold serial dilutions of viral samples in serum free DMEM. After 1.5 h incubation, 1ml of 1.25% methylcellulose containing 2% FBS was added into each well. After incubation for 4 days, cells were fixed with 4% buffered formalin, and stained with 0.5% crystal violet. Plaque morphology and numbers were recorded after rinsing the plates with deionized water.

Immunostaining focus assay was carried out following a previously described protocol (12) with modifications. In brief, Vero cells at 80% confluence in 24-well plates were inoculated with 100μl of 10-fold serial dilutions of viral samples. After 1.5 h

incubation, 1ml of 1.25% methylcellulose containing 2% FBS was added into each well. Cells were incubated at 37 °C for 7 d before being fixed in methanol–acetone (1:1) fixation solution. After fixation, the cells were incubated with ZIKV-specific HMAF, followed by incubation with goat anti-mouse IgG conjugated with horseradish peroxidase (HRP) as a secondary antibody. Finally, viral foci were detected by the addition of DAB (3, 3 -diaminobenzidine) HRP substrate, following the manufacturer's instructions (Enhanced HRP-DAB kit, Tiangen, China).

Indirect immunofluorescence assays (IFA). The cells infected with ZIKVs were washed once with phosphate-buffered saline (PBS) and fixed by cold (-20°C) 5% acetic acid in acetone for 15 min at room temperature (RT). The fixed cells were washed with PBS three times and incubated with a 4G2 mouse monoclonal antibody (mAb) that is cross-reactive with flavivirus E protein (ATCC) (diluted 1:200) for 1 h. After three rinses with PBS, the cells were incubated with goat anti-mouse IgG conjugated to FITC (Proteintech, Wuhan, China) at a 1:200 dilution with PBS at RT for 1h. After three rinses with PBS, cell nuclei were stained with Hoechst 33258. The fluorescent signal images were taken with a NIKON fluorescence microscope (Tokyo, Japan).

Animal Immunization. AG6 mice deficient in type I and II interferon (IFN α/β/γ) receptors were gifts from Qibin Leng (Institute Pasteur of Shanghai, Chinese Academy of Sciences), and were bred in specific-pathogen-free conditions in the Animal Resource Center at the Wuhan Institute of Virology, Chinese Academy of Sciences. 4-week-old AG6 mice were infected with 10^4, 10^3, 10^2, 10^1, or 10^0 PFU WT or mutant viruses through intraperitoneal (ip) injection. PBS was injected into the mock-infected mice through the same route. The clinical course of the viral infection was monitored by survival, weight loss, and disease symptoms. The lethal dose 50% (LD50) for each

ZIKVs was determined using the method of Reed and Muench (66). On 3 and 6 dpi, to measure viremia, serum samples were collected from anesthetized mice and clarified by centrifugation for 5 minutes at 3000 g. On 3, 7 14, and 28dpi, heart, liver, spleen, lung, kidney, brain, testes, eye, ovary, uterus, intestine and muscle of the immunized mice were removed, weighed and homogenized with zirconia beads in 1ml of TRIzol Reagent. Then, quantification of viral load in samples was performed using qRT-PCR. On 28 dpi, the immunized mice were challenged through the i.p. route with 10^4 IFU of ZIKVwt, and measured for viremia on day 2 after challenge. On day 14 after challenge, all the mice were anesthetized, bled for the titration of neutralize antibody, and sacrificed.

Quantitative real-time RT-PCR assays. Total RNA was extracted from cell supernatants, sera or organs using TRIzol Reagent, and reverse transcribed by using PrimeScript™ RT reagent kit. A universal pair of primers (67) (forward primer, AARTACACATACCARAACAAAGTG, and reverse primer TCCRCTCCCYCTYTGGTCTTG) was used to amplify the region of 9378-9479 in the NS5 gene which is preserved in all virus strains. All quantitative real-time PCR (qRT-PCR) assays were performed with SYBR Green Master Mix (Bio-Rad) on the CFX96 touch real-time PCR detection system (Bio-Rad). Cycling conditions were as follows: 95°C for 3 min, followed by 40 cycles of 95°C for 10 sec, 55°C for 10 sec, and 65°C for 45 sec. The ZIKVwt NS5 gene was utilized as a standard and was cloned into pGEM-T (Promega, WI, USA). Log dilutions of the DNA standard were included with each RT-PCR assay. Virus concentration was determined by interpolation onto the curve made up of 10-fold serial dilutions of the standards.

Immunohistochemistry. Tissues were fixed in 4% formaldehyde at 4 °C for 24h and embedded in paraffin. For IHC, the paraffin-embedded tissues were sectioned at a

thickness of 5 µm and mounted on slides. After being heated at 60 °C for 1 h, the slides were deparaffinized with xylene, and were then cleared with alcohol. After antigen retrieval, the sections were incubated with an anti-ZIKV envelope (E) protein monoclonal antibodies (mAb) (BioFront Technologies, Fl, USA, 1:100 dilution) overnight at 4 °C. Following incubation overnight with the antibodies, a goat anti-mouse IgG conjugated with HRP was applied to each slide. Visualization was acquired with the DAB reagent (DAKO, Envision System kit). The sections were also stained with hematoxylin and eosin. Images were acquired by the whole-slide digital Pannoramic scanner (3D-Histech, Budapest, Hungary)

$PRNT_{50}$. 50% Plaque Reduction Neutralization Test ($PRNT_{50}$) was developed for measuring ZIKV-specific neutralizing antibodies according to a previously described protocol (14) with modifications. Briefly, heat-inactivated serum samples were two-fold serially diluted, and incubated with 100 PFU ZIKVwt at 37°C for 1.5 h. Then, the virus–serum mixture (200 µl) was added to Vero cells at 80% confluence in 12-well plates. After incubation at 37°C for 1.5h, 1.25% methyl cellulose overlay was added and plates were incubated for 4 days at 37 °C in 5% CO_2. Then, the cells were fixed with 4% formalin and stained with 0.5% crystal violet. Plaque morphology and numbers were recorded after rinsing the plates with deionized water. $PRNT_{50}$ titer was expressed as the reciprocal of the highest dilution of each serum sample that caused a 50% reduction in the plaque number relative to the control samples. Samples with titer of ≥10 were considered as seropositive.

ELISPOT assay. The splenocytes were isolated by mouse lymphocyte separation medium (DAKEWEI, Beijing China) on 28 dpi, and adjusted to a concentration of 5×10^6 cells/ml in complete RPMI-1640 medium. The production of IFN-γ was measured using

an ELISPOT assay according to the manufacturer's instructions (DAKEWEI). Briefly, 96-well PVDF plates (Millipore, Bedford, MA) were pre-coated with anti-mouse IFN-γ. Then, 100μl of lymphocytes was added to the wells in triplicate, stimulated with heat-inactivated ZIKV (10^6IFU/well), along with RPMI 1640 medium alone (as negative control) or ConA (5μg/ml, Sigma, positive control). Following the 20 h incubation at 37°C, the lymphocytes were removed, and 100 μl of biotinylated anti-mouse IFN-γ was added and incubated at 37°C for 1 h. Following washing, the plate was incubated with properly diluted Streptavidin-HRP conjugate solution at 37°C for 1 h. Finally, 100 μl of AEC substrate solution was added and incubated at RT for 25 min in the dark. The plate was stopped by washing with demineralized water, air-dried and read using an ELISPOT reader (Bioreader 4000; Bio-sys, Germany). The numbers of spot-forming cells (SFC) per 5×10^5 cells were calculated. Medium backgrounds were consistently <10 SFC per 5×10^5cells.

Statistical Analysis. The Student's t-test and ANOVA test were used to analyze all the virologic and immunologic data if there were significant differences ($p < 0.05$). The statistical analyses were performed in IBM SPSS Statistics v18.0 (Chicago, IL, USA).

ACKNOWLEDGMENTS

The authors thank Prof. Qibin Leng in the Institute Pasteur of Shanghai, Chinese Academy of Sciences for providing AG6 mice. This work was supported by the National Key R&D Program of China (2016YFD0500406), the National Natural Science Foundation of China (NSFC) (NO. 81471953) and Youth Innovation Promotion Association of CAS (2016302). The funders had no role in study design, data collection and interpretation, or the decision to submit the work for publication.

REFERENCES

1. Hamel R, Dejarnac O, Wichit S, Ekchariyawat P, Neyret A, Luplertlop N, Perera-Lecoin M, Surasombatpattana P, Talignani L, Thomas F, Cao-Lormeau VM, Choumet V, Briant L, Despres P, Amara A, Yssel H, Misse D. 2015. Biology of Zika Virus Infection in Human Skin Cells. J Virol 89:8880-96.
2. Dick GW, Kitchen SF, Haddow AJ. 1952. Zika virus. I. Isolations and serological specificity. Trans R Soc Trop Med Hyg 46:509-20.
3. Dowall SD, Graham VA, Rayner E, Atkinson B, Hall G, Watson RJ, Bosworth A, Bonney LC, Kitchen S, Hewson R. 2016. A Susceptible Mouse Model for Zika Virus Infection. PLoS Negl Trop Dis 10:e0004658.
4. Zhao H, Fernandez E, Dowd KA, Speer SD, Platt DJ, Gorman MJ, Govero J, Nelson CA, Pierson TC, Diamond MS, Fremont DH. 2016. Structural Basis of Zika Virus-Specific Antibody Protection. Cell 166:1016-27.
5. Song BH, Yun SI, Woolley M, Lee YM. 2017. Zika virus: History, epidemiology, transmission, and clinical presentation. J Neuroimmunol doi:10.1016/j.jneuroim.2017.03.001.
6. Duffy MR, Chen TH, Hancock WT, Powers AM, Kool JL, Lanciotti RS, Pretrick M, Marfel M, Holzbauer S, Dubray C, Guillaumot L, Griggs A, Bel M, Lambert AJ, Laven J, Kosoy O, Panella A, Biggerstaff BJ, Fischer M, Hayes EB. 2009. Zika virus outbreak on Yap Island, Federated States of Micronesia. N Engl J Med 360:2536-43.
7. Mlakar J, Korva M, Tul N, Popovic M, Poljsak-Prijatelj M, Mraz J, Kolenc M, Resman Rus K, Vesnaver Vipotnik T, Fabjan Vodusek V, Vizjak A, Pizem J, Petrovec M, Avsic Zupanc T. 2016. Zika Virus Associated with Microcephaly. N Engl J Med 374:951-8.
8. Morrison TE, Diamond MS. 2017. Animal Models of Zika Virus Infection, Pathogenesis, and Immunity. J Virol 91.
9. D'Ortenzio E, Matheron S, Yazdanpanah Y, de Lamballerie X, Hubert B, Piorkowski G, Maquart M, Descamps D, Damond F, Leparc-Goffart I. 2016. Evidence of Sexual Transmission of Zika Virus. N

Engl J Med 374:2195-8.

10. Sumathy K, Kulkarni B, Gondu RK, Ponnuru SK, Bonguram N, Eligeti R, Gadiyaram S, Praturi U, Chougule B, Karunakaran L, Ella KM. 2017. Protective efficacy of Zika vaccine in AG129 mouse model. Sci Rep 7:46375.

11. Abbink P, Larocca RA, De La Barrera RA, Bricault CA, Moseley ET, Boyd M, Kirilova M, Li Z, Ng'ang'a D, Nanayakkara O, Nityanandam R, Mercado NB, Borducchi EN, Agarwal A, Brinkman AL, Cabral C, Chandrashekar A, Giglio PB, Jetton D, Jimenez J, Lee BC, Mojta S, Molloy K, Shetty M, Neubauer GH, Stephenson KE, Peron JP, Zanotto PM, Misamore J, Finneyfrock B, Lewis MG, Alter G, Modjarrad K, Jarman RG, Eckels KH, Michael NL, Thomas SJ, Barouch DH. 2016. Protective efficacy of multiple vaccine platforms against Zika virus challenge in rhesus monkeys. Science 353:1129-32.

12. Shan C, Muruato AE, Nunes BT, Luo H, Xie X, Medeiros DB, Wakamiya M, Tesh RB, Barrett AD, Wang T, Weaver SC, Vasconcelos PF, Rossi SL, Shi PY. 2017. A live-attenuated Zika virus vaccine candidate induces sterilizing immunity in mouse models. Nat Med doi:10.1038/nm.4322.

13. Richner JM, Himansu S, Dowd KA, Butler SL, Salazar V, Fox JM, Julander JG, Tang WW, Shresta S, Pierson TC, Ciaramella G, Diamond MS. 2017. Modified mRNA Vaccines Protect against Zika Virus Infection. Cell 168:1114-1125.e10.

14. Pardi N, Hogan MJ, Pelc RS, Muramatsu H, Andersen H, DeMaso CR, Dowd KA, Sutherland LL, Scearce RM, Parks R, Wagner W, Granados A, Greenhouse J, Walker M, Willis E, Yu JS, McGee CE, Sempowski GD, Mui BL, Tam YK, Huang YJ, Vanlandingham D, Holmes VM, Balachandran H, Sahu S, Lifton M, Higgs S, Hensley SE, Madden TD, Hope MJ, Kariko K, Santra S, Graham BS, Lewis MG, Pierson TC, Haynes BF, Weissman D. 2017. Zika virus protection by a single low-dose nucleoside-modified mRNA vaccination. Nature 543:248-251.

15. Chahal JS, Fang T, Woodham AW, Khan OF, Ling J, Anderson DG, Ploegh HL. 2017. An RNA nanoparticle vaccine against Zika virus elicits antibody and CD8+ T cell responses in a mouse model. Scientific Reports 7:252.

16. Larocca RA, Abbink P, Peron JP, Zanotto PM, Iampietro MJ, Badamchi-Zadeh A, Boyd M, Ng'ang'a

D, Kirilova M, Nityanandam R, Mercado NB, Li Z, Moseley ET, Bricault CA, Borducchi EN, Giglio PB, Jetton D, Neubauer G, Nkolola JP, Maxfield LF, De La Barrera RA, Jarman RG, Eckels KH, Michael NL, Thomas SJ, Barouch DH. 2016. Vaccine protection against Zika virus from Brazil. Nature 536:474-8.

17. Dowd KA, Ko SY, Morabito KM, Yang ES, Pelc RS, DeMaso CR, Castilho LR, Abbink P, Boyd M, Nityanandam R, Gordon DN, Gallagher JR, Chen X, Todd JP, Tsybovsky Y, Harris A, Huang YS, Higgs S, Vanlandingham DL, Andersen H, Lewis MG, De La Barrera R, Eckels KH, Jarman RG, Nason MC, Barouch DH, Roederer M, Kong WP, Mascola JR, Pierson TC, Graham BS. 2016. Rapid development of a DNA vaccine for Zika virus. Science 354:237-240.

18. Boigard H, Alimova A, Martin GR, Katz A, Gottlieb P, Galarza JM. 2017. Zika virus-like particle (VLP) based vaccine. PLoS Neglected Tropical Diseases 11:e0005608.

19. Garg H, Sedano M, Plata G, Punke EB, Joshi A. 2017. Development of Virus-Like-Particle Vaccine and Reporter Assay for Zika Virus. J Virol 91.

20. Shan C, Xie X, Muruato Antonio E, Rossi Shannan L, Roundy Christopher M, Azar Sasha R, Yang Y, Tesh Robert B, Bourne N, Barrett Alan D, Vasilakis N, Weaver Scott C, Shi P-Y. 2016. An Infectious cDNA Clone of Zika Virus to Study Viral Virulence, Mosquito Transmission, and Antiviral Inhibitors. Cell Host & Microbe 19:891-900.

21. Xie X, Zou J, Shan C, Yang Y, Kum DB, Dallmeier K, Neyts J, Shi PY. 2016. Zika Virus Replicons for Drug Discovery. EBioMedicine 12:156-160.

22. Yun SI, Lee YM. 2017. Zika virus: An emerging flavivirus. J Microbiol 55:204-219.

23. Annamalai AS, Pattnaik A, Sahoo BR, Muthukrishnan E, Natarajan SK, Steffen D, Vu HLX, Delhon G, Osorio FA, Petro TM, Xiang SH, Pattnaik AK. 2017. Zika Virus Encoding Non-Glycosylated Envelope Protein is Attenuated and Defective in Neuroinvasion. J Virol doi:10.1128/jvi.01348-17.

24. Fontes-Garfias CR, Shan C, Luo H, Muruato AE, Medeiros DBA, Mays E, Xie X, Zou J, Roundy CM, Wakamiya M, Rossi SL, Wang T, Weaver SC, Shi P-Y. 2017. Functional analysis of glycosylation of Zika virus envelope protein. Cell reports 21:1180-1190.

25. Hilgenfeld R. 2016. Zika virus NS1, a pathogenicity factor with many faces. The EMBO Journal

35:2631-2633.

26. Wang D, Chen C, Liu S, Zhou H, Yang K, Zhao Q, Ji X, Chen C, Xie W, Wang Z, Mi L-Z, Yang H. 2017. A Mutation Identified in Neonatal Microcephaly Destabilizes Zika Virus NS1 Assembly in Vitro. Scientific Reports 7:42580.

27. Coleman JR, Papamichail D, Skiena S, Futcher B, Wimmer E, Mueller S. 2008. Virus attenuation by genome-scale changes in codon pair bias. Science 320:1784-7.

28. Shen SH, Stauft CB, Gorbatsevych O, Song Y, Ward CB, Yurovsky A, Mueller S, Futcher B, Wimmer E. 2015. Large-scale recoding of an arbovirus genome to rebalance its insect versus mammalian preference. Proc Natl Acad Sci U S A 112:4749-54.

29. Gutman GA, Hatfield GW. 1989. Nonrandom utilization of codon pairs in Escherichia coli. Proc Natl Acad Sci U S A 86:3699-703.

30. Wang B, Yang C, Tekes G, Mueller S, Paul A, Whelan SP, Wimmer E. 2015. Recoding of the vesicular stomatitis virus L gene by computer-aided design provides a live, attenuated vaccine candidate. MBio 6.

31. Le Nouen C, Brock LG, Luongo C, McCarty T, Yang L, Mehedi M, Wimmer E, Mueller S, Collins PL, Buchholz UJ, DiNapoli JM. 2014. Attenuation of human respiratory syncytial virus by genome-scale codon-pair deoptimization. Proc Natl Acad Sci U S A 111:13169-74.

32. Meng J, Lee S, Hotard AL, Moore ML. 2014. Refining the balance of attenuation and immunogenicity of respiratory syncytial virus by targeted codon deoptimization of virulence genes. MBio 5:e01704-14.

33. Nogales A, Baker SF, Ortiz-Riano E, Dewhurst S, Topham DJ, Martinez-Sobrido L. 2014. Influenza A virus attenuation by codon deoptimization of the NS gene for vaccine development. J Virol 88:10525-40.

34. Mueller S, Coleman JR, Wimmer E. 2009. Putting synthesis into biology: a viral view of genetic engineering through de novo gene and genome synthesis. Chem Biol 16:337-47.

35. Le Nouen C, McCarty T, Brown M, Smith ML, Lleras R, Dolan MA, Mehedi M, Yang L, Luongo C, Liang B, Munir S, DiNapoli JM, Mueller S, Wimmer E, Collins PL, Buchholz UJ. 2017. Genetic

stability of genome-scale deoptimized RNA virus vaccine candidates under selective pressure. Proc Natl Acad Sci U S A 114:E386-e395.

36. Martínez MA, Jordan-Paiz A, Franco S, Nevot M. 2016. Synonymous Virus Genome Recoding as a Tool to Impact Viral Fitness. Trends in Microbiology 24:134-147.

37. Beutler E, Gelbart T, Han JH, Koziol JA, Beutler B. 1989. Evolution of the genome and the genetic code: selection at the dinucleotide level by methylation and polyribonucleotide cleavage. Proc Natl Acad Sci U S A 86:192-6.

38. Burge C, Campbell AM, Karlin S. 1992. Over- and under-representation of short oligonucleotides in DNA sequences. Proc Natl Acad Sci U S A 89:1358-62.

39. Rima BK, McFerran NV. 1997. Dinucleotide and stop codon frequencies in single-stranded RNA viruses. J Gen Virol 78 (Pt 11):2859-70.

40. Karlin S, Doerfler W, Cardon LR. 1994. Why is CpG suppressed in the genomes of virtually all small eukaryotic viruses but not in those of large eukaryotic viruses? J Virol 68:2889-97.

41. Burns CC, Campagnoli R, Shaw J, Vincent A, Jorba J, Kew O. 2009. Genetic Inactivation of Poliovirus Infectivity by Increasing the Frequencies of CpG and UpA Dinucleotides within and across Synonymous Capsid Region Codons. Journal of Virology 83:9957-9969.

42. Al-Saif M, Khabar KS. 2012. UU/UA dinucleotide frequency reduction in coding regions results in increased mRNA stability and protein expression. Mol Ther 20:954-9.

43. Burns CC, Shaw J, Campagnoli R, Jorba J, Vincent A, Quay J, Kew O. 2006. Modulation of Poliovirus Replicative Fitness in HeLa Cells by Deoptimization of Synonymous Codon Usage in the Capsid Region. Journal of Virology 80:3259-3272.

44. Mueller S, Papamichail D, Coleman JR, Skiena S, Wimmer E. 2006. Reduction of the rate of poliovirus protein synthesis through large-scale codon deoptimization causes attenuation of viral virulence by lowering specific infectivity. J Virol 80:9687-96.

45. Cheng BY, Ortiz-Riano E, Nogales A, de la Torre JC, Martinez-Sobrido L. 2015. Development of live-attenuated arenavirus vaccines based on codon deoptimization. J Virol 89:3523-33.

46. Diaz-San Segundo F, Medina GN, Ramirez-Medina E, Velazquez-Salinas L, Koster M, Grubman MJ,

de los Santos T. 2015. Synonymous Deoptimization of Foot-and-Mouth Disease Virus Causes Attenuation In Vivo while Inducing a Strong Neutralizing Antibody Response. J Virol 90:1298-310.

47. Yang C, Skiena S, Futcher B, Mueller S, Wimmer E. 2013. Deliberate reduction of hemagglutinin and neuraminidase expression of influenza virus leads to an ultraprotective live vaccine in mice. Proc Natl Acad Sci U S A 110:9481-6.

48. Mueller S, Coleman JR, Papamichail D, Ward CB, Nimnual A, Futcher B, Skiena S, Wimmer E. 2010. Live attenuated influenza virus vaccines by computer-aided rational design. Nat Biotechnol 28:723-6.

49. Ni YY, Zhao Z, Opriessnig T, Subramaniam S, Zhou L, Cao D, Cao Q, Yang H, Meng XJ. 2014. Computer-aided codon-pairs deoptimization of the major envelope GP5 gene attenuates porcine reproductive and respiratory syndrome virus. Virology 450-451:132-9.

50. Li XF, Dong HL, Wang HJ, Huang XY, Qiu YF, Ji X, Ye Q, Li C, Liu Y, Deng YQ. 2018. Development of a chimeric Zika vaccine using a licensed live-attenuated flavivirus vaccine as backbone. Nature Communications.

51. Broadbent AJ, Santos CP, Anafu A, Wimmer E, Mueller S, Subbarao K. 2016. Evaluation of the attenuation, immunogenicity, and efficacy of a live virus vaccine generated by codon-pair bias de-optimization of the 2009 pandemic H1N1 influenza virus, in ferrets. Vaccine 34:563-70.

52. Fros JJ, Dietrich I, Alshaikhahmed K, Passchier TC, Evans DJ, Simmonds P. 2017. CpG and UpA dinucleotides in both coding and non-coding regions of echovirus 7 inhibit replication initiation post-entry. eLife 6:e29112.

53. Takata MA, Gonçalves-Carneiro D, Zang TM, Soll SJ, York A, Blanco-Melo D, Bieniasz PD. 2017. CG dinucleotide suppression enables antiviral defence targeting non-self RNA. Nature 550:124.

54. Gaunt E, Wise HM, Zhang H, Lee LN, Atkinson NJ, Nicol MQ, Highton AJ, Klenerman P, Beard PM, Dutia BM, Digard P, Simmonds P. 2016. Elevation of CpG frequencies in influenza A genome attenuates pathogenicity but enhances host response to infection. eLife 5:e12735.

55. Kunec D, Osterrieder N. 2016. Codon Pair Bias Is a Direct Consequence of Dinucleotide Bias. Cell Reports 14:55-67.

688 56. Tulloch F, Atkinson NJ, Evans DJ, Ryan MD, Simmonds P. 2014. RNA virus attenuation by codon
689 pair deoptimisation is an artefact of increases in CpG/UpA dinucleotide frequencies. Elife
690 3:e04531.
691 57. Futcher B, Gorbatsevych O, Shen SH, Stauft CB, Song Y, Wang B, Leatherwood J, Gardin J, Yurovsky
692 A, Mueller S, Wimmer E. 2015. Reply to Simmonds et al.: Codon pair and dinucleotide bias have
693 not been functionally distinguished. Proceedings of the National Academy of Sciences of the
694 United States of America 112:E3635-E3636.
695 58. Aliota MT, Caine EA, Walker EC, Larkin KE, Camacho E, Osorio JE. 2016. Characterization of Lethal
696 Zika Virus Infection in AG129 Mice. PLoS Negl Trop Dis 10:e0004682.
697 59. Rossi SL, Tesh RB, Azar SR, Muruato AE, Hanley KA, Auguste AJ, Langsjoen RM, Paessler S,
698 Vasilakis N, Weaver SC. 2016. Characterization of a Novel Murine Model to Study Zika Virus. Am J
699 Trop Med Hyg 94:1362-9.
700 60. Weger-Lucarelli J, Duggal NK, Bullard-Feibelman K, Veselinovic M, Romo H, Nguyen C, Ruckert C,
701 Brault AC, Bowen RA, Stenglein M, Geiss BJ, Ebel GD. 2017. Development and Characterization of
702 Recombinant Virus Generated from a New World Zika Virus Infectious Clone. J Virol 91.
703 61. Yuan L, Huang XY, Liu ZY, Zhang F, Zhu XL, Yu JY, Ji X, Xu YP, Li G, Li C, Wang HJ, Deng YQ, Wu M,
704 Cheng ML, Ye Q, Xie DY, Li XF, Wang X, Shi W, Hu B, Shi PY, Xu Z, Qin CF. 2017. A single mutation in
705 the prM protein of Zika virus contributes to fetal microcephaly. Science
706 doi:10.1126/science.aam7120.
707 62. Ma W, Li S, Ma S, Jia L, Zhang F, Zhang Y, Zhang J, Wong G, Zhang S, Lu X, Liu M, Yan J, Li W, Qin C,
708 Han D, Qin C, Wang N, Li X, Gao GF. 2016. Zika Virus Causes Testis Damage and Leads to Male
709 Infertility in Mice. Cell 167:1511-1524.e10.
710 63. Schuster P, Fontana W, Stadler PF, Hofacker IL. 1994. From sequences to shapes and back: a case
711 study in RNA secondary structures. Proc Biol Sci 255:279-84.
712 64. Deng C, Liu S, Zhang Q, Xu M, Zhang H, Gu D, Shi L, He J, Xiao G, Zhang B. 2016. Isolation and
713 characterization of Zika virus imported to China using C6/36 mosquito cells. Virol Sin 31:176-9.
714 65. Schwarz MC, Sourisseau M, Espino MM, Gray ES, Chambers MT, Tortorella D, Evans MJ. 2016.

715 Rescue of the 1947 Zika Virus Prototype Strain with a Cytomegalovirus Promoter-Driven cDNA
716 Clone. mSphere 1.
717 66. Reed L. 1938. A simple method of estimating fifty per cent endprints. Am J Hyg 27:493-497.
718 67. Faye O, Faye O, Diallo D, Diallo M, Weidmann M, Sall AA. 2013. Quantitative real-time PCR
719 detection of Zika virus and evaluation with field-caught mosquitoes. Virol J 10:311.

720

Figure legends

Fig 1. Construction of the infectious cDNA clone of ZIKVwt and generation of codon pair-deoptimized ZIKVs.

(A) The strategy for constructing the full-length cDNA clone of ZIKVwt. Four cDNA fragments from A to D that cover the complete ZIKV genome were synthesized from viral RNA using RT-PCR, and sequentially cloned into the plasmid pACYC177 to form the full-length cDNA clone of ZIKV (ZIKVwt-FL). CMV promoter, HDVr/SV40 polyA, and the position of relevant restriction sites are shown. (B) Gene maps of the codon pair-deoptimized ZIKVs Min E, Min NS1, and Min E+NS1. Codon pair-deoptimized genes are shown as white boxes; WT E gene is shown as orange box; WT NS1 gene is shown as blue box. Restriction sites (KpnI and ClaI) used for the constructions are indicated.

Fig 2. Replication of WT and codon pair-deoptimized ZIKVs in cell culture.

Vero cells (A and B) or C6/36 cells (C and D) were infected with viruses at an moi of 0.01. Viral loads were determined by qRT-PCR (A and C), and virus titers were measured by immunostaining focus assay on Vero cells (B and D). (E and F) Growth properties of viruses were determined by passaging them on Vero cells at an moi of 0.01. (G) Plaque-size phenotype on Vero cells of virus variants, visualized by immunostaining following incubation for 4 d (WT and Min NS1) and 7 d (Min E and Min E+NS1) under methylcellulose at 37 °C, respectively. Data shown (a, b, c, d, e and f) are the means and standard deviations (mean ± SD) analyzed by Student's t test (two tailed, *, $P < 0.05$; **, $P < 0.01$; ***, $P < 0.001$).

Fig 3. IFA of E protein expression in Vero cells infected with WT or codon pair-deoptimized ZIKVs.

744 Vero cells were infected with viruses at an moi of 0.01. On 2, 3 and 4 dpi, IFA was
745 performed as described in Materials and Methods. All the images were captured at
746 10×magnification. Green represents E protein and blue represents nuclei (stained with
747 Hoechst 33258).

748 **Fig 4. Attenuation of codon pair-deoptimized ZIKVs in AG6 mice**

749 Groups of AG6 mice (3-to-4-week-old, n = 6) were infected intraperitoneally with 10^2
750 IFU of WT or codon pair-deoptimized ZIKVs, respectively. Body weight loss (A) and
751 survival (B) were monitored daily for 4 weeks. Mice were euthanized when they lost 25%
752 of their initial body weight.

753 **Fig 5. Immunohistochemical staining of E protein in brain sections from infected**
754 **mice.**

755 AG6 mice were infected with 102 IFU of viruses (n=3). The brain tissues from mice
756 infected with WT virus were collected at 7 dpi. The brain tissues from mice infected with
757 Min E+NS1 were collected at 28 dpi.

758 **Fig 6. Viral loads in organs or sera of infected AG6 mice.**

759 Mice (n = 3) were infected with 10^2 IFU of viruses, euthanized at day 3, day 6, or day 7,
760 and organ viral loads were determined at day 3 and day 7 by qRT-PCR (A) and
761 Immunostaining focus assay (spleen； B). Serum viral loads were determined at day 3
762 and day 6 by qRT-PCR (C). Data shown (a, b and c) are the means and standard
763 deviations (mean ± SD) analyzed by Student's t test (two tailed, *, $P < 0.05$; **, $P < 0.01$;
764 ***, $P < 0.001$).

765 **Fig 7. Humoral and cellular immune responses induced by codon pair-deoptimized**
766 **ZIKVs in mice.**

(A) Prechallenge neutralization antibody titers were measured on day 28 (day 7 for WT virus) after immunization using a standard $PRNT_{50}$ assay. (B) Cellular immune responses were assessed on day 28 after immunization by IFN-γ ELISPOT assays. Data shown (a and b) are the means and standard deviations (mean ± SD) analyzed by Student's t test (two tailed, **, $P < 0.01$).

Fig 8. Protection efficacy of codon pair-deoptimized ZIKVs in mice.

Mice were immunized with 10^2 IFU of codon pair-deoptimized viruses or mock vaccinated with PBS. At 4 weeks postvaccination, animals were challenged with 10^4 IFU of WT virus (an approximately 5500-fold MLD50). Body weight loss (A) and survival (B) were evaluated for 14 days after the challenge. Mice were euthanized when they lost 25% of their initial body weight. (C) Postchallenge viremia was quantified by qRT-PCR on day 3 after challenge. (D) Postchallenge neutralization antibody titers were determined at day 14 after challenge by a standard $PRNT_{50}$ assay. Data shown (c and d) are the means and standard deviations (mean ± SD) analyzed by Student's t test (two tailed, *, $P < 0.05$; **, $P < 0.01$; ***, $P < 0.001$).

Fig 9. Min E+NS1 immunization protected AG6 mice during pregnancy.

(A) Scheme of immunization of 4-week-old AG6 female mice with 10^2 IFU of Min E+NS1 or PBS. (B-D) At day 32 post immunization, vaccinated female mice were mated with AG6 males. Pregnant mice (n = 4) were with 10^4 IFU of WT virus on E6. (B) Neutralization antibody titers were measured on day 1 before challenge using a standard $PRNT_{50}$ assay. (C) Maternal viremia on day 2 after challenge was quantified by qRT-PCR. (D) Outcome of fetuses from Min E+NS1 or PBS vaccinated dams. [a] All PBS-immunized pregnant mice died without delivery. [b] Maternal neutralization antibody titers of pups delivered at term to Min E+NS1 vaccinated dams were measured at the 21th day

after birth. Data shown (b and c) are the means and standard deviations (mean ± SD) analyzed by Student's t test (two tailed, ***, $P < 0.001$).

Table legends

Table 1. Characteristics of deoptimized ZIKV genome segments.

Table 2. The increases of C3G1 and U3A1 in deoptimized ZIKV genome segments.

Table 3. Median lethal dose (MLD50) values in AG6 mice after intraperitoneal inoculation.

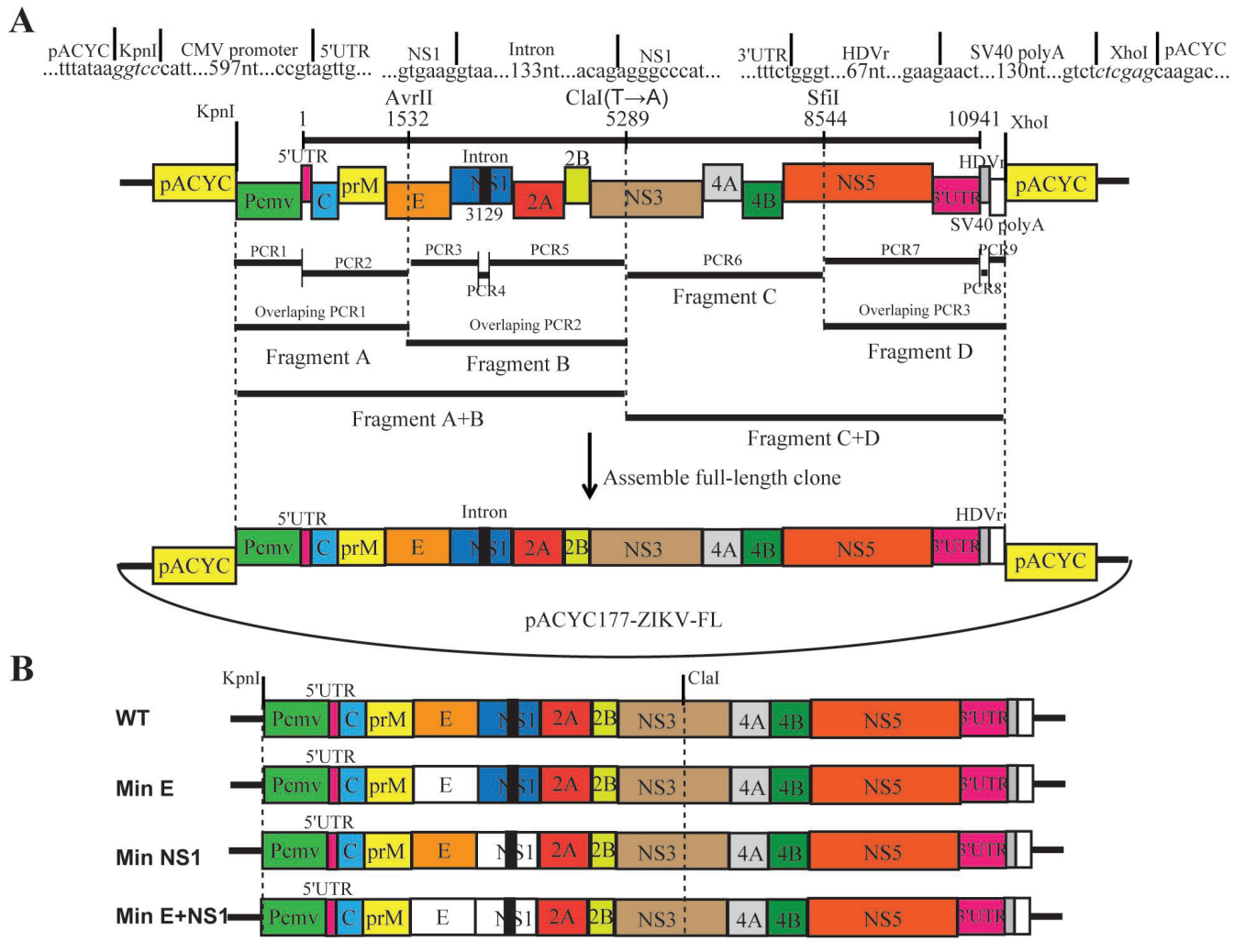

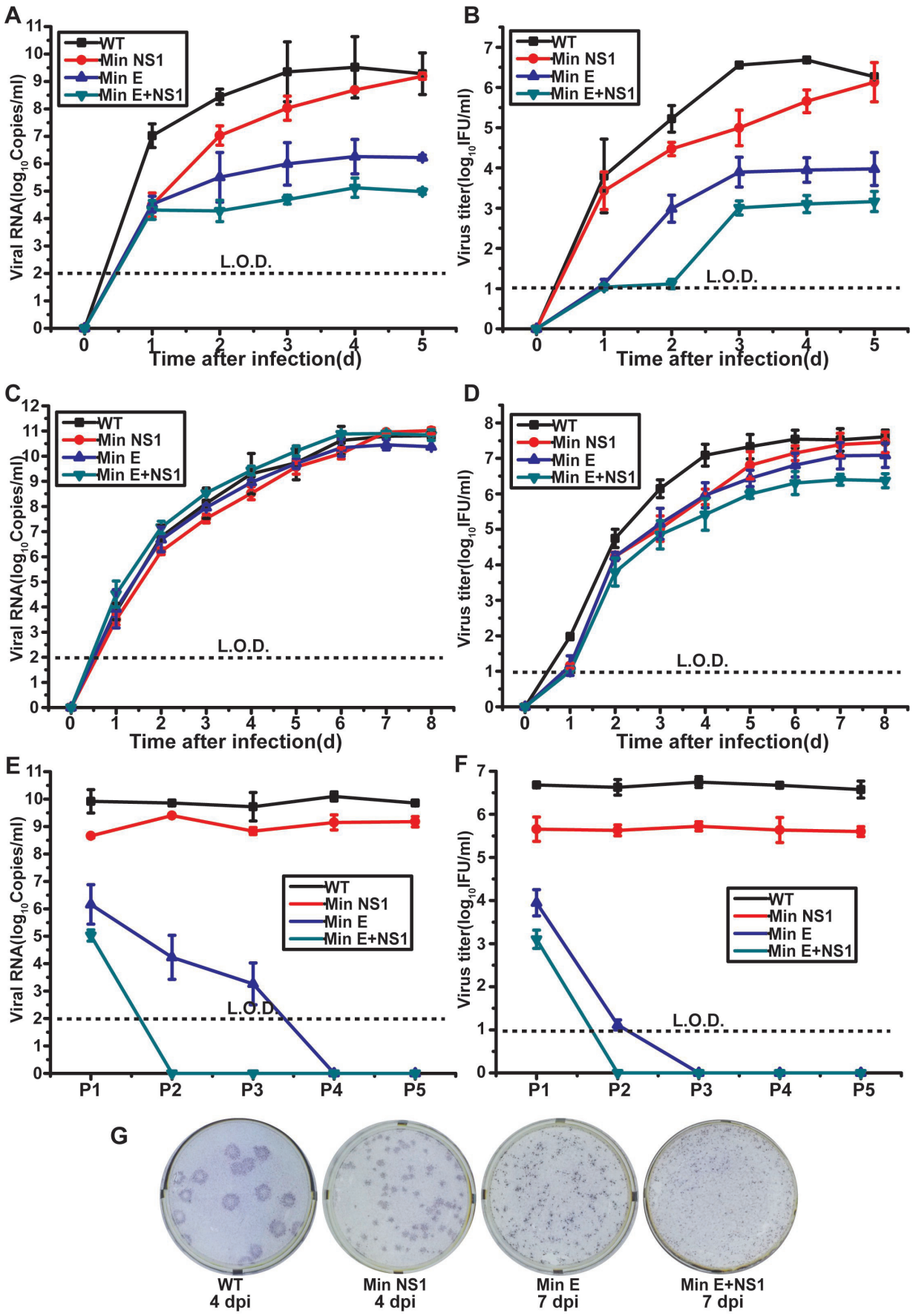

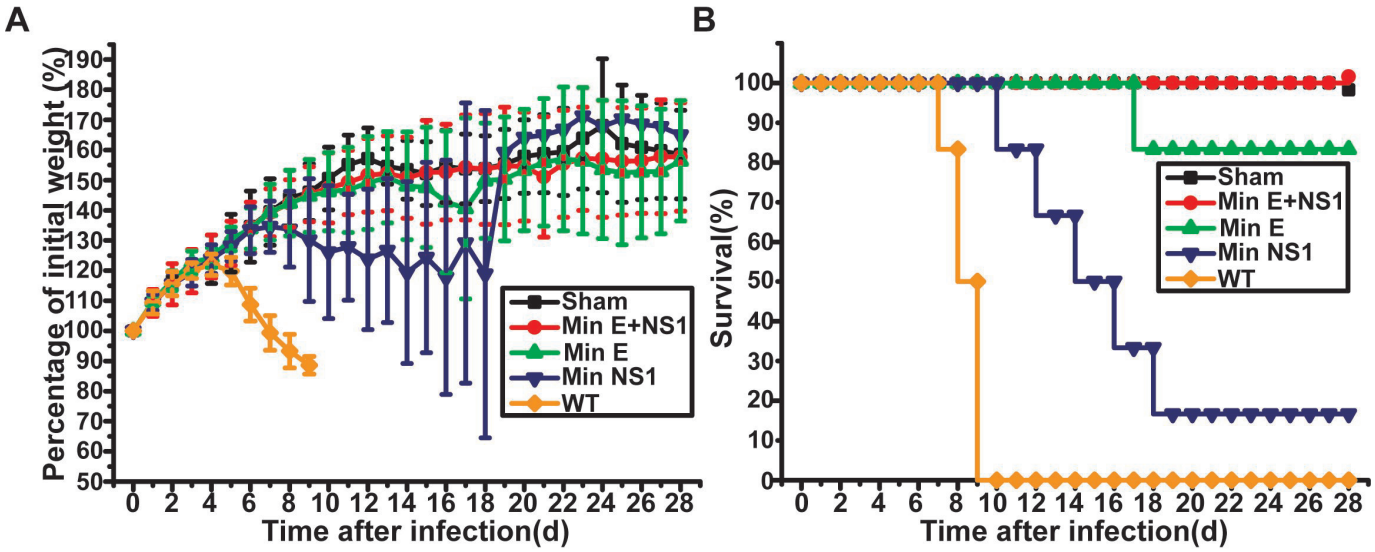

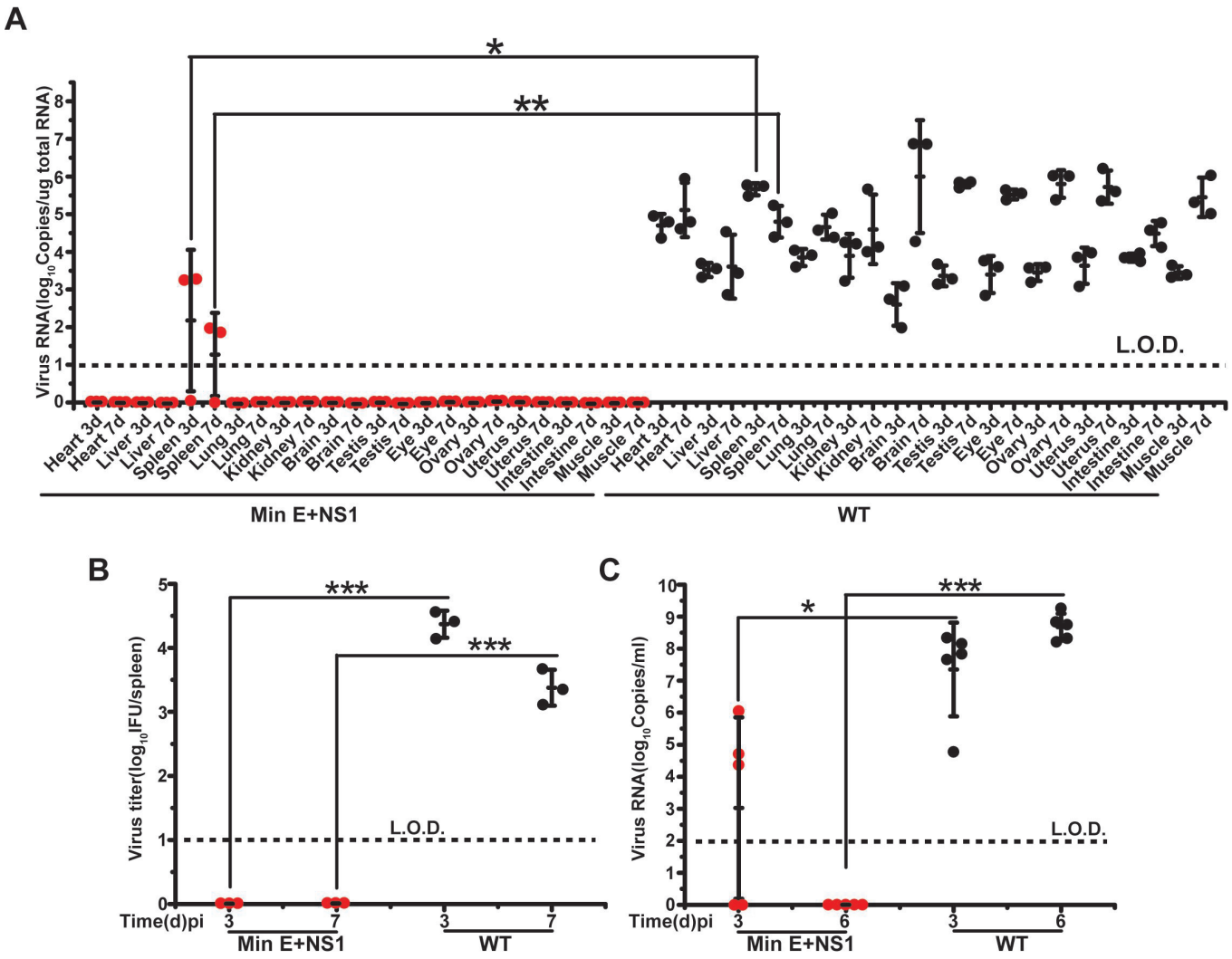

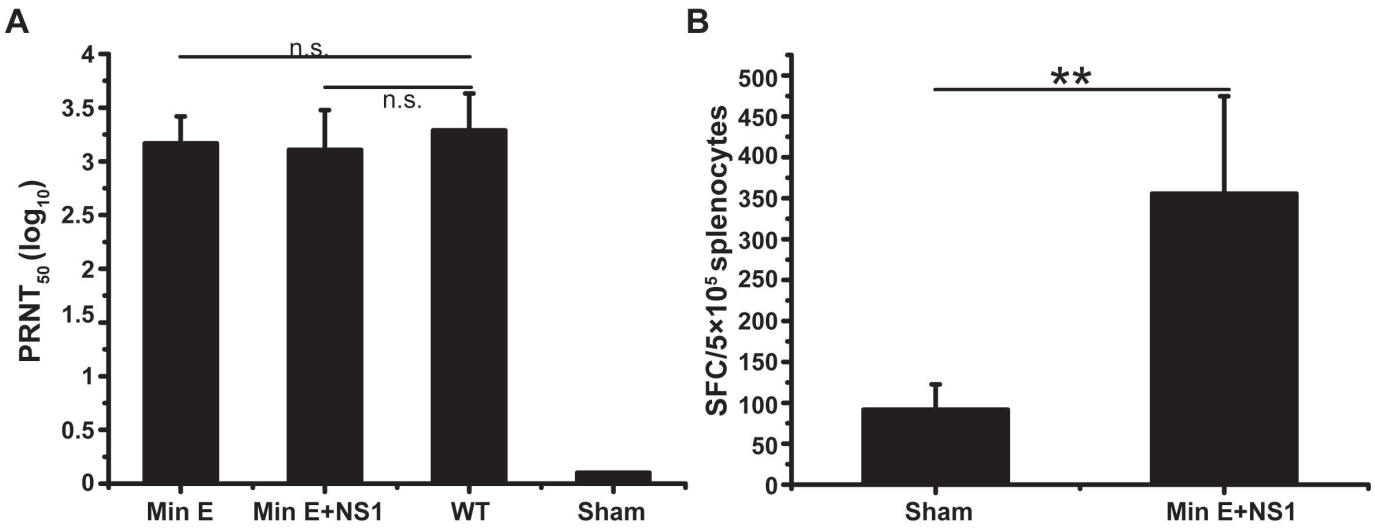

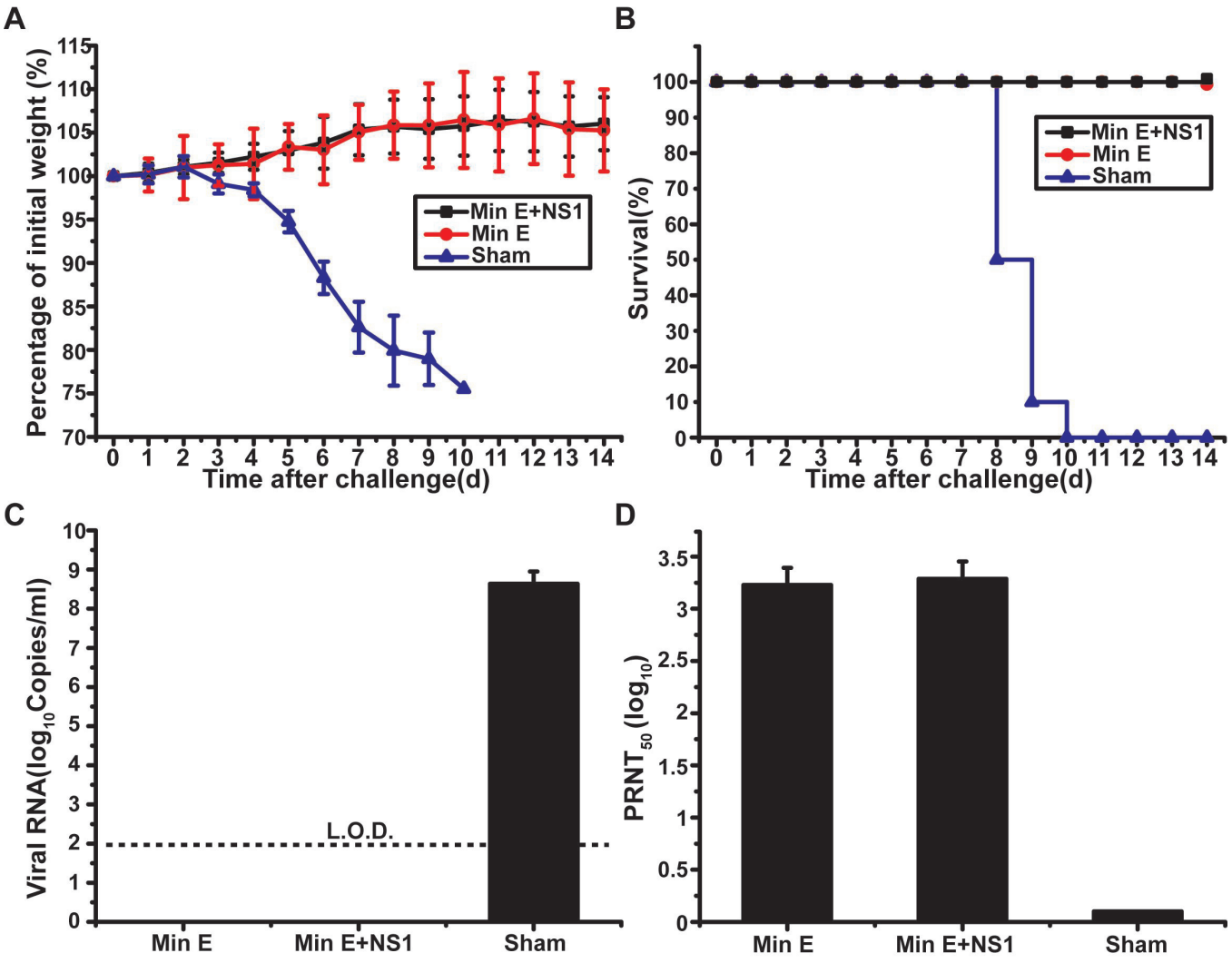

Journal of Virology
JVI
Journal of Virology

A

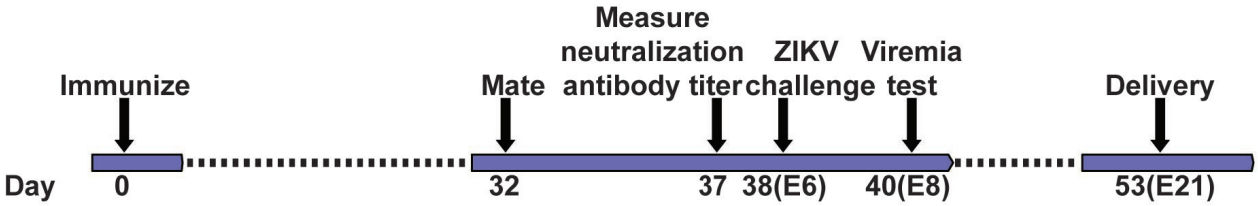

B

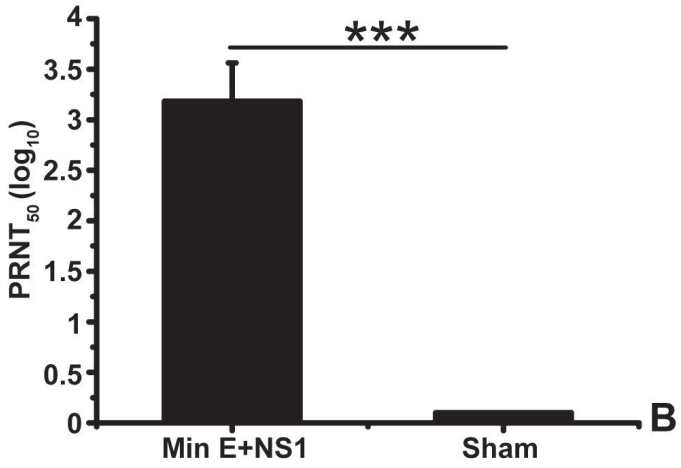

C

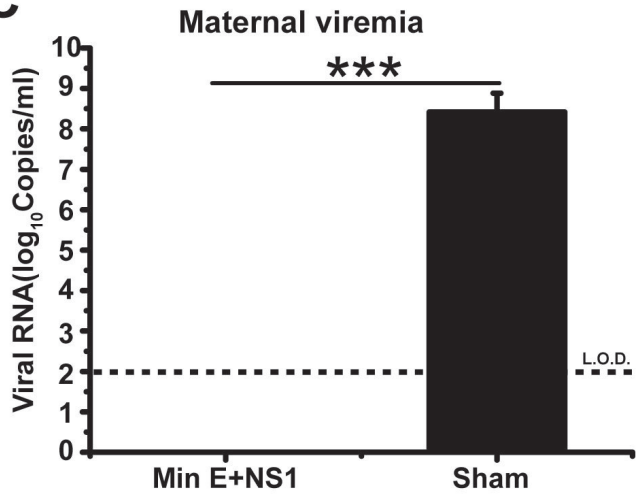

D

Group	Delivery	Pups	
		Health	maternal antibody level
Sham	No(n=4)[a]	—	—
Min E+NS1	Yes(n=4)	Yes	160 ± 74.1[b]

Table 1. Characteristics of deoptimized ZIKV genome segments

Virus	Deoptimized coding region	Human codon pair bias of wt segment	Human codon pair bias of deoptimized segment	Mosquito codon pair bias of wt segment	Mosquito codon pair bias of deoptimized segment	Number of silent mutations (total nucleic acids)
Min E	1-1512	0.0336	-0.5741	-0.0099	-0.0729	363(1512)
Min NS1	1-1056	0.0059	-0.5162	-0.0077	-0.0809	219(1056)
Min E+NS1	1-2568	0.0222	-0.5503	-0.0090	-0.0764	582(2568)

Table 2. The increases of C_3G_1 and U_3A_1 in deoptimized ZIKV genome segments

Gene	Encoding	Length, nt	C3G1	ΔC3G1*	U3A1	ΔU3A1*
E	WT	1512	20	—	14	—
E	deoptimized	1512	111	+91(455%)	66	+52(371%)
NS1	WT	1056	17	—	13	—
NS1	deoptimized	1056	67	+50(294%)	37	+24(185%)
E+NS1	WT	2568	37	—	27	—
E+NS1	deoptimized	2568	178	+141(381%)	103	+76(281%)

*The number of CpGs and UpAs in deoptimized segments is added with respect to WT segments.

Table 3. Median lethal dose (MLD50) values in AG6 mice after intraperitoneal inoculation

Virus	MLD50 (no. of PFU/mouse)
ZIKVwt	1.78
Min E	1750.83
Min NS1	2.98
Min E+NS1	3981.07